Steady-State and Frequency Response of a Thin-Film Heat Flux Gauge

Christopher S. Cho*
Western Michigan University, Kalamazoo, Michigan 49008
and
Gustave C. Fralick[†] and Hemanshu D. Bhatt[‡]
NASA Lewis Research Center, Cleveland, Ohio 44135

A new and simpler design of thin-film heat flux gauge has been developed for use in high-heat-flux environments. Heat flux gauges of the same design were fabricated on three different substrates and tested. The heat flux gauge comprises a thermopile and a thermocouple junction, which measures the surface temperature. The thermopile has 40 pairs of S-type thermocouples and is covered by two thermal resistance layers. Calibration and testing of these gauges were first carried out in an arc-lamp calibration facility. Sensitivity of the gauge was discussed in terms of the relative conductivity and surface temperature. The heat flux calculated from the gauge output was in good agreement with the precalibrated standard sensor. The steady-state and the transient response characteristics of the heat flux gauge were also investigated using a carbon dioxide pulse laser as a heat source. The dynamic frequency response was evaluated in terms of the nondimensional amplitude ratio with respect to the frequency spectrum of a chopped laser beam. The frequency response of the gauge was determined to be about 3 kHz. The temperature profiles in the thin-film heat flux gauge were obtained numerically in steady-state conditions using FLUENT and compared with the experimental results.

Nomenclature

d = thickness of thermal resistance layer, m
E_s = thermopile voltage output, mV
K = thermal conductivity, W/m°C
K/α = relative conductivity, W/m°C
N = number of thermocouple pairs in the thermopile
Q = heat flux, W/m^2
$S(T)$ = absolute thermoelectric power at temperature T, mV/°C
T = temperature, °C
t = time, s
α = absorptivity
Δd = thickness difference in thermal resistance layers between 1 and 2

Subscripts

1, 2 = thermal resistance layers 1 and 2, respectively

Introduction

DESIGN of a high-speed flight system requires an accurate knowledge of steady-state and transient heat loading conditions. One of the severe problems in high Mach number flight is the high local heat transfer due to the viscous interaction and the shock interaction.[1] The development of an aeropropulsion system requires the measurement of the surface distribution of parameters such as pressure, temperature, and heat transfer rate. To measure the rate of incident heat flux, various types of heat flux gauges have been developed. Conventional heat flux gauges can be categorized as 1) gauges based on the temperature difference measurement, which include the Gardon-type gauge,[2] the Schmidt–Boelter gauge,[3] and standard layered gauges[4]; 2) gauges based on transient surface temperature measurement using various techniques such as coaxial thermocouples[5] and thin-film resistance elements[6]; and 3) gauges based on the dissipation of electrical power from a heater mounted on the substrate surface.[7] One of the major drawbacks of the conventional heat flux gauge is a distortion of thermal- and flow-fields created due to the sensor's very presence. Other limitations of these sensors include poor response to transient heat flux and limited high-temperature or high-heat-flux measurement capabilities. A miniature plug-type heat flux gauge was developed to measure the heat flux in the turbine blade of a Space Shuttle's main engine.[8] A simple gradient fluxmeter and a multiple gradient fluxmeter, which were usable up to 1000°C, were developed.[9]

The thin-film heat flux gauge offers a unique solution to most of these limitations associated with the conventional heat flux gauges. The operating principle of a thin-film heat flux gauge is similar to that of the layered gauge, which involves a measurement of the temperature difference across a thermal resistance layer. The incident heat flux is directly proportional to the temperature difference across the thermal resistance layer. Because the temperature drop is very small, the differential output is increased by placing a number of thermocouple pairs connected in series to form a thermopile. Thin-film gauges offer many advantages over conventional gauges: capability to measure steady-state as well as transient heat fluxes, excellent transient response, minimal obstruction to fluid flow, high-temperature capability, and good sensitivity due to large output signal. Several types of thin-film heat flux gauges have been developed to achieve high spatial resolution and fast temperature response. Will[10] developed a thin-film heat flux gauge that had an array of thermocouples on the upper and lower surfaces of a thin insulating layer to achieve an accurate and fast transient response. It had 20 elements of platinum vs platinum–10% rhodium thermocouple pairs on a silicon dioxide insulating layer. Bhatt and Fralick[11] designed a new thin-film heat flux sensor for use in a high-heat flux environment.

The frequency response of a heat flux gauge is one of the important characteristics to be considered for the measurement of a fast transient heat transfer rate. Two types of thin-film heat flux gauges that had frequency responses of 50 kHz and 250 Hz, respectively, were developed.[12] Further, a frequency response characteristic of the heat flux gauge in the range of 100 kHz was reported.[13]

The objective of the current research is to measure the magnitude of incident heat flux and to determine the frequency response of the novel thin-film heat flux gauge. This new and simpler design was developed to reduce the complexity in fabrication as encountered

in the previous version of the heat flux gauge.[10] This paper introduces a new design of heat flux gauges whose operation is based on the temperature gradient created by thickness difference in two thermal resistance layers. The testing and calibration of the gauge is also described. To validate the design, the same configuration of thermopiles was fabricated on three different types of substrate materials: Al_2O_3, Inconel 100®, and silicon nitride. Thermopiles fabricated on Al_2O_3 and Inconel 100 substrates were used for calibration and sensitivity measurement. After validation of the design, a thermopile fabricated on the silicon nitride substrate was tested for the frequency response characteristics. Numerically, the thin-film heat flux gauge was simulated in a two-dimensional model and solved to obtain the temperature profiles. Steady-state and transient response characteristics of the thin-film heat flux gauges are investigated and will be discussed in the following section.

Design of Thin-Film Heat Flux Gauge

A novel thin-film heat flux gauge has been developed to achieve fast response in transient heat transfer. Most thin-film heat flux gauges have two thermocouple junctions installed separately across a thermal resistance layer. The incident heat flux is measured by a temperature gradient across the thermal resistance layer.

In this newly designed thin-film heat flux gauge, thermocouple junctions are placed on the same plane but separated in a radial direction (Fig. 1). The temperature difference is created by introducing different thicknesses of thermal resistance layers at two different radii. Silicon dioxide was used for the two thermal resistance layers. To create a large emf output, 40 pairs of Pt–Pt/10%Rh (type S) thermocouples are connected in series to form a thermopile. The thermopile is fabricated in a circular pattern on the substrate using rf sputter deposition.

Thermopile output was read between leg A and leg C (shown in Fig. 1). Another new thermocouple junction was constructed outside the thermopile to read the surface temperature of the heat flux gauge. The surface temperature was measured between leg A and leg B.

The cross-sectional view of the heat flux gauge is shown in Fig. 2. The substrate had dimensions of 30×30 mm base area and 2.4-mm
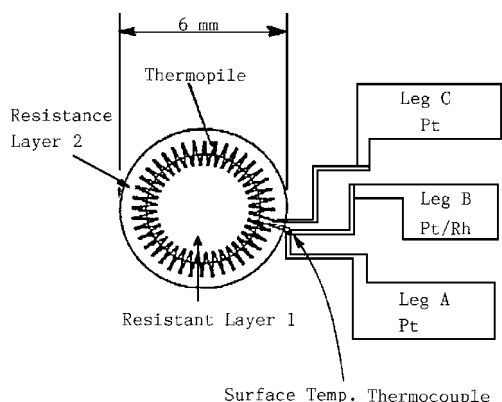

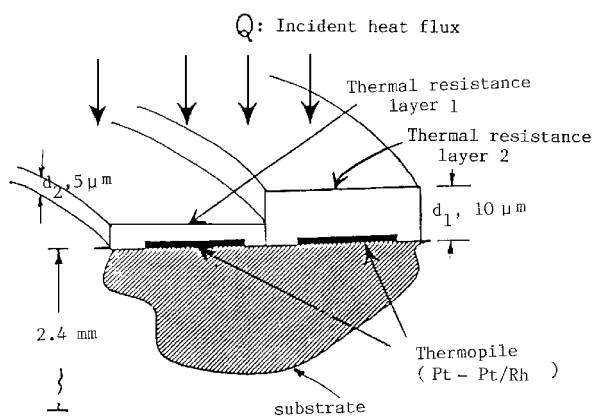**Fig. 1   Design layout of the thin-film heat flux gauge.**

Fig. 2   Cross-sectional view of the heat flux gauge.

thickness. The thermocouple junctions were located at the inner and outer circumferences of the thermopile geometry, which had radii of 1.5 and 2.5 mm, respectively, from the center of the thermopile.

After the thermopile was fabricated on the substrate surface, two different thicknesses of SiO_2 thermal resistance layers were deposited over the thermopile (Fig. 2). The inner circumference of the thermopile had a thermal resistance layer 5 μm thick. The outer circumference of the thermopile had a thermal resistance layer 10 μm thick. Two different thicknesses of thermal resistance layers were chosen to create a temperature gradient in the direction normal to the thermal resistance layer.

When a uniform heat flux is applied on the surface of the heat flux gauge, a temperature gradient develops inside the thermal resistance layer according to Fourier's conduction law. The temperature difference measured by the thermopile is a function of the thickness of the thermal resistance layer and of the radial distance between the inner and outer thermocouple junctions. Therefore, the radially separated thermocouple pairs read the two-dimensional temperature gradient. As indicated later in the numerical solution, the major portion of the temperature gradient is created in the radial direction, whereas the minor portion of temperature gradient is created in a direction normal to the thermal resistance layer. But a simple exercise[11] shows that the thermopile output is directly proportional to the incident heat flux and to the difference in thickness of the thermal resistance layers as indicated in the following equation:

$$Q = \frac{K}{(d_1 - d_2)} \cdot (T_1 - T_2) \quad (1)$$

Heat Flux Gauge Calibration

Calibration is an essential requirement for the accurate determination of the incident heat flux magnitude. Most calibration systems are based on radiation or conduction. Calibration using conduction yields accurate results but is limited to relatively low values of heat fluxes. Though radiation can be used to produce a wide range of heat flux values, this technique has drawbacks such as requiring a calibration of the standard sensor. A typical calibration procedure involves the exposure of the test sensor as well as the precalibrated standard sensor to the same heat flux. The heat flux determined by the standard sensor output is then used to determine the sensitivity of the new gauge. Using this procedure, the sensitivity can be found as a function of incident heat flux and many other operating parameters.

The gauges fabricated on Al_2O_3 and Inconel 100 substrates were calibrated using the Vortek arc-lamp[14] calibration facility at NASA Lewis Research Center. The arc lamp can produce repeatable, uniform heat fluxes in the range of 0.02–5 MW/m^2. The heat flux to which the gauges were exposed could be varied by changing the input current to the arc lamp, as well as by changing the distance of the sensor from the arc lamp. Gauges fabricated both on Al_2O_3 substrate and on Inconel 100 substrate were mounted in front of the arc lamp using a Macor® glass-ceramic holder. The gauges were mounted at a distance of 12 cm and centered with respect to the arc lamp. The incident heat flux was changed by varying the lamp current from 50 to 300 A. The voltages from the thermopile and the surface thermocouple were measured at a rate of 10 Hz. The heat flux values were also measured by using the Hy-Cal gauges.[15] Figure 3 shows the output from the thermopile and surface thermocouple for the thin-film gauge on an Al_2O_3 substrate.

As seen in Fig. 3, the output voltages from both the surface thermocouple and the thermopile increased as a function of time. The surface thermocouple output increased due to the constant radiative heating during the test. The heat flux output of the gauge increased although the heat flux value was constant during the test. This behavior can be explained by the change in absolute thermoelectric power of the thermopile and the thermophysical properties of the resistance layer with changing temperature. The sensor fabricated on Al_2O_3 substrate failed after 20 s during the test at lamp current of 200 A. The sensor fabricated on the Inconel 100 survived the testing at lamp current of 300 A corresponding to surface temperature of about 800°C.
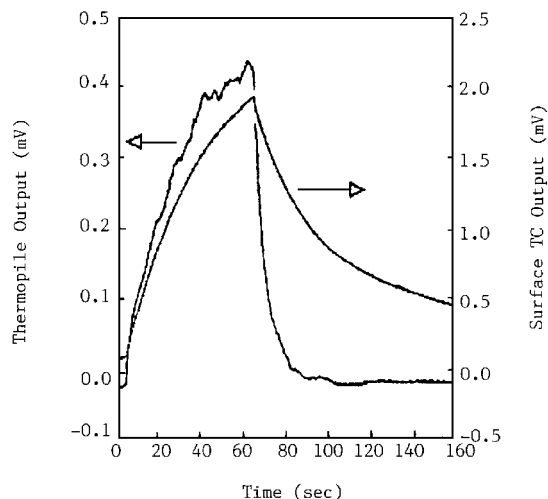
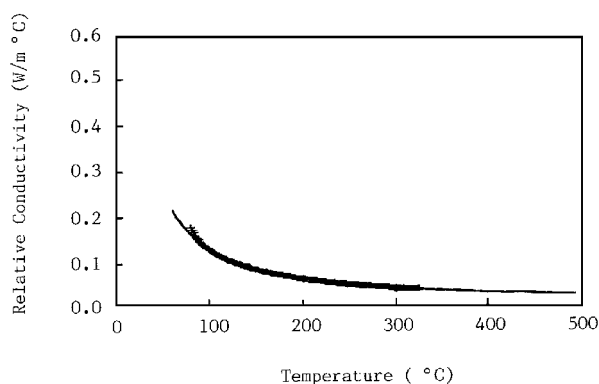Fig. 3 Output of thin-film gauge on Al₂O₃ for the test at lamp current of 100 A.

Fig. 4 Relative conductivity K/α calculated for gauge on Al₂O₃ using the gauge output data at 150 A.

Fig. 5 Calculated heat flux as a function of time during testing at 50 A for gauge on Al₂O₃ substrate.

Fig. 6 Comparison of average heat flux values at different lamp currents for precalibrated Hy-Cal gauge and thin-film heat flux gauge.

A novel approach was used to determine the sensitivity of the thin-film heat flux sensors. The incident heat flux on the heat flux gauge at steady state is given by

$$Q \cdot \alpha(T) = K(T) \cdot (\Delta T / \Delta d) \qquad (2)$$

The thermopile output E_s is given by

$$E_s = N \cdot S(T) \cdot \Delta T \qquad (3)$$

These equations can be rearranged in term of the incident heat flux Q,

$$Q = \frac{K(T)}{\alpha(T)} \cdot \frac{E_s}{N \cdot S(T) \cdot \Delta d} \qquad (4)$$

Kreider[16] reported that, after 50 h operation at 750°C, the Seebeck coefficient of a platinum/10% rhodium element was reduced 50% compared to the as-sputtered condition. In the current experiment, the exposure time of the thermocouples to the incident heat flux was of the order of minutes. Therefore, it is reasonable to assume that the thin-film surface thermocouple behaves similarly to a wire thermocouple. The surface temperature of the thin-film gauge during testing can be determined using the standard thermoelectric power tables.

Because the temperatures in the thermal resistance layers are unknown, the temperature from the surface thermocouple is considered as a reference temperature for the sensitivity analysis. At this reference surface temperature, the corresponding thermopile output E_s is evaluated from Fig. 4, and the values of $K(T)$ and $\alpha(T)$ are obtained. In Eq. (4), the parameters N and Δd can be determined because they depend on the gauge geometry. The values of $K(T)/\alpha(T)$ in Eq. (4) are defined as the relative conductivity and are plotted in Fig. 4. Once the relative conductivity is determined
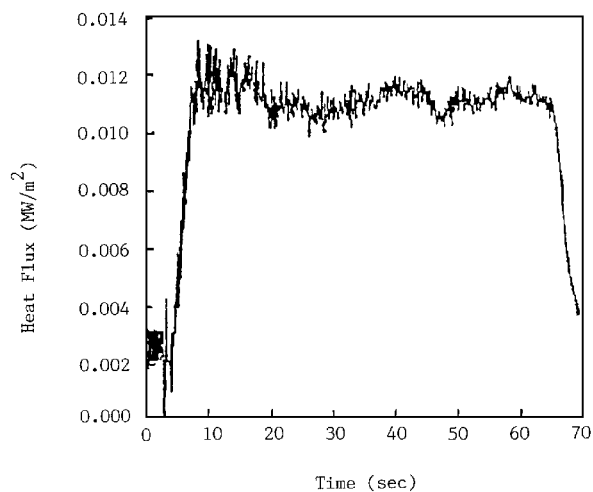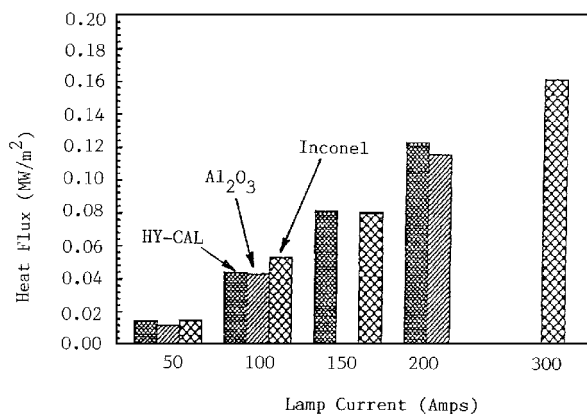
as a function of temperature, it can be curvefitted and extrapolated over the whole temperature range.

Using the relative conductivity, the incident heat flux Q can be calculated with respect to the heat flux gauge output E_s, according to Eq. (4). What one achieves from this exercise is the decoupling of the temperature behavior in the gauge and the material parameters as compared to using a single calibration factor in a conventional calibration procedure. If the relative conductivity plotted in Fig. 4 is rearranged using the concept presented in Eq. (4), the sensitivity Q/E_s can be presented as a function of surface temperature.

Figure 5 shows a typical plot of the heat flux as a function of time calculated using the just-described calibration technique. It is observed from Fig. 5 that the heat flux increases rapidly with the increase in lamp current and stabilizes to an approximately constant value.

Figure 6 compares the heat flux values calculated for the thin-film heat flux gauges to the values determined by the precalibrated standard sensor for the corresponding same lamp currents. In Fig. 6, the heat flux values calculated for the thin-film gauges are in good agreement with the values determined by the precalibrated standard sensor. This indicates that the heat flux measurement capability relies on the configuration of the gauge geometry rather than a selection of the substrate materials.

Experimental Setup

The thin-film heat flux gauge was tested using a CO₂ laser as a constant heat flux source. The experiments were done in a room-temperature environment. The CO₂ laser had maximum power output of 150 W. It was chosen as a constant heat flux source due to the flexibility in controlling its power level. The CO₂ laser had a wavelength of 10.6 μm, which is in the infrared region. The laser
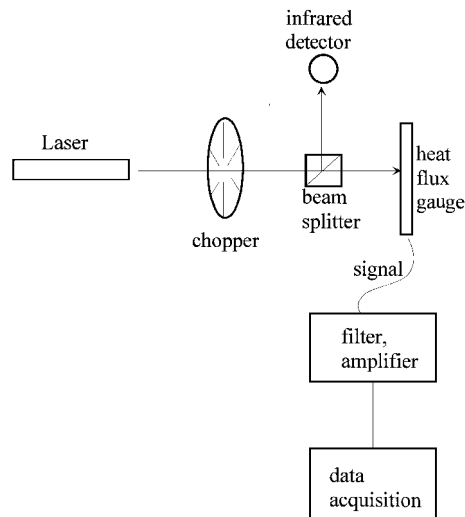
Fig. 7 Schematic diagram of test setup.

Fig. 8a Steady-state response of delta-T during heating period , $Q =$ 0.324 MW/m^2.

Fig. 8b Steady-state response of surface temperature during heating period.

beam diameter was originally 6 mm but was expanded to 12 mm to cover the entire thermopile. The beam was directed normal to the heat flux gauge.

The schematic diagram of the test setup is shown in Fig. 7. The test setup consists of a CO_2 laser, a mechanical chopper, a beam splitter, an infrared detector, a water-cooled power meter, a heat flux gauge, and a data acquisition system including antialiasing signal filters and amplifiers. Two types of tests were performed using the given test setup: long-time (steady-state) response of the heat flux gauge until the heat flux gauge reached the steady state and the frequency response (transient response) of the heat flux gauge. For the steady-state response test, the chopper was not used. The heat flux gauge was heated continuously until its output reached steady state, and then the laser was turned off to test the cooling characteristics of the heat flux gauge.

The radiative properties of the thermal resistance layers and the substrate determine the amount of heat flux absorbed by the gauge. The absorptivity of silicon nitride is sensitive to the wavelength. Experimental data by Touloukian and Ho[17] show that the absorptivity of the silicon nitride ranges from 0.2 to 0.7 in the wavelength between 6 and 14 μm. For the CO_2 laser wavelength of 10.6 μm, the absorptivity of 0.4 was chosen. The emissivity of silicon dioxide is determined to be 0.4 based on the reported results.[10]

During the tests, three levels of excitation voltages were selected to control the laser power. The equivalent heat flux levels for the CO_2 laser power were 0.473, 0.810, and 1.048 MW/m^2 corresponding to the 12-mm beam diameter. Because the absorptivities were chosen to be 0.4, the absorbed heat flux by the gauge was assumed to be 40% of the incident CO_2 laser power. The corresponding absorbed heat fluxes by the heat flux gauge were 0.189, 0.324, and 0.419 MW/m^2, respectively.

The temperature difference (delta-T) across the thermal resistance layer was measured by the thermopile. The voltage output from the thermopile was amplified 1000 times and sent to the data acquisition system. The sampling rate of the A/D data acquisition system was controlled between 500 and 10,000 Hz. Measurements were taken for the heating period, the combined heating and cooling period, and the cooling period.

Steady-State Response of Heat Flux Gauge

To measure the steady-state output of the heat flux gauge, the laser beam was irradiated on the heat flux gauge until the heat flux gauge reached steady state. After that heating period, the gauge was allowed to cool until it reached the ambient temperature. Two parameters, the delta-T from the thermopile and the surface temperature, were measured.

Figure 8a shows the measurement results during 150 s of a heating period. The two curves in Fig. 8a represent the experimental results as well as the numerical calculation results. Although it is not clearly noticeable in Fig. 8a, the obtained data indicate the following: during
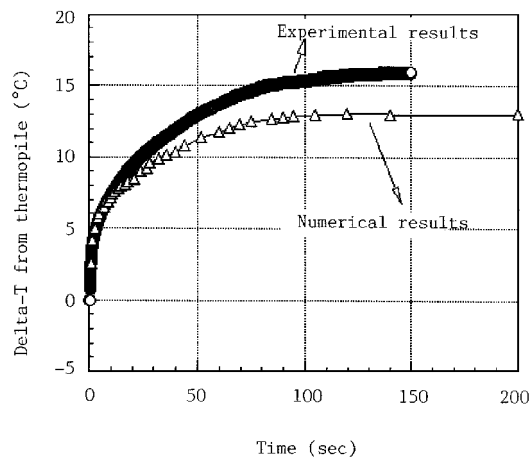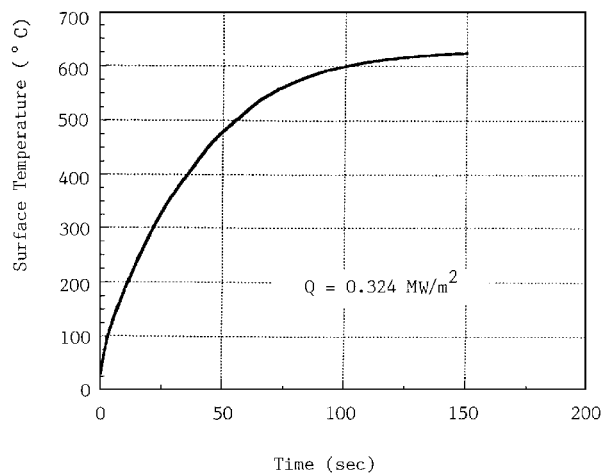
the initial heating period the delta-T rose suddenly as a step function within less than $\frac{1}{10}$ of a second and then gradually increased following a logarithmic curve. It is believed that the initial steep rise of temperature was caused by the instant temperature gradient created by the thickness difference in the thermal resistance layer. The gradual increase in delta-T was caused by the radial distribution of the incident heat flux in the substrate. It suggests that the temperature rise comprises two components that are in the direction normal to the heat flux gauge and in the direction of radial distribution of the heat flux. A measurement of the surface temperature for 150 s is shown in Fig. 8b.

The time constant of the heat flux gauge was obtained from Figs. 8a and 8b by taking the corresponding rise time when the temperature change becomes $1/e$ from the steady-state temperature. In this approach, the time constant during the heating process was about 30 s. The time constant is an indicator of the steady-state performance, but it does not explain the transient behavior of the heat flux gauge that will be evaluated in the later section. The heat flux gauge survived the repeated tests of heating and cooling for a temperature of 650°C.

Figures 9a and 9b show the measured surface temperature and the delta-T during the combined heating and cooling process. The heat flux gauge was heated for 15 s and allowed to cool for a subsequent 15 s. During the cooling process a sharp decrease of delta-T was observed within a second, but the surface temperature showed a gradual temperature decrease to reach the ambient temperature, as shown in Figs. 9a and 9b. The slope of the cooling curve, which represents the sensitivity, is much flatter in Fig. 9b than the slope shown in Fig. 9a. The results in Figs. 9a and 9b follow the same trend as observed in Fig. 3 during the calibration process, which validates the performance of the thin-film heat flux gauge.
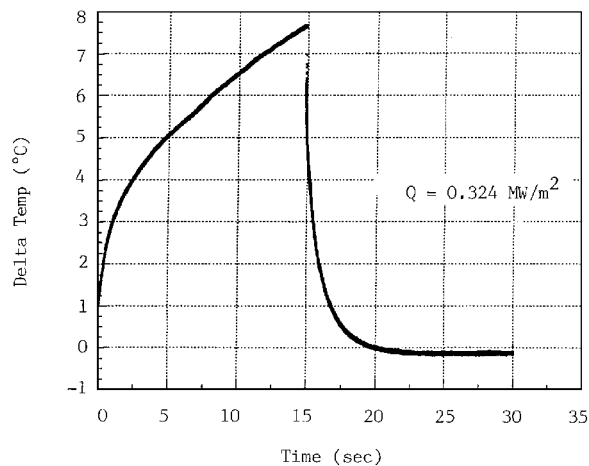
Fig. 9a Steady-state response of delta-T during the combined heating and cooling period.
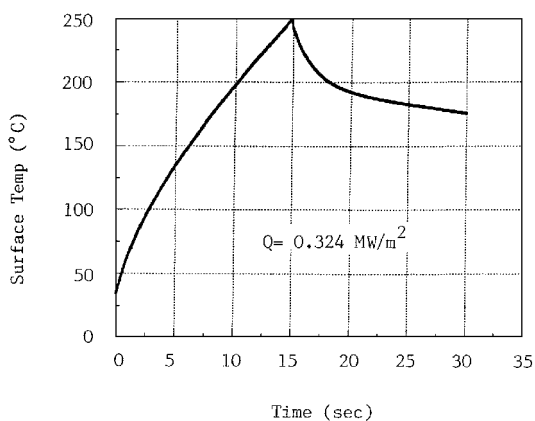

Fig. 9b Steady-state response of the surface temperature during the combined heating and cooling period.

Computational Simulation of the Steady-State Response Using FLUENT

The thin-film heat flux gauge was simulated using FLUENT, a commercially available computational thermal–fluid software package developed by the Creare Company. Figure 10 shows the dimensions of the numerical model used in the two-dimensional modeling of the thin-film heat flux gauge. A grid size of 151×61, nonuniform in the X and Y directions, was used in the modeling.

The following boundary conditions were considered for the numerical simulation.

1) A constant heat flux of 0.324 MW/m^2 was applied on the 6-mm-radius surface of the thin-film heat flux gauge. A symmetry boundary condition was assumed at the left surface.

2) The material properties such as the thermal conductivity and the specific heat capacity of the heat flux gauge were treated as functions of the temperature. The material properties were expressed in terms of temperature using piecewise equations.

3) The surface of the heat flux gauge was assumed to be exposed to both the convection cooling and the radiation cooling. The absorptivity was chosen to be 0.4 (Refs. 10 and 17).

4) The thermopile 40 pairs of Pt–Pt/10%Rh thermocouples were simulated as a 1-μm-thick platinum disk, which was placed between the substrate surface and the thermal resistance layer.

The temperature profiles were obtained from the computational simulation under the constant heat flux level of 0.324 MW/m^2. Figure 11a shows the temperature distribution obtained in the heat flux gauge when $t = 1.0$ s. In Fig. 11a, the surface temperature at location E, which corresponded to the surface thermocouple location, was 61.33°C. That calculated temperature was very close to the experimentally measured data. The enlarged view of temperature profile in the thermopile region is shown in Fig. 11b.

The locations of the thermocouple junctions in the thermopile are labeled as A and B in Fig. 11b.
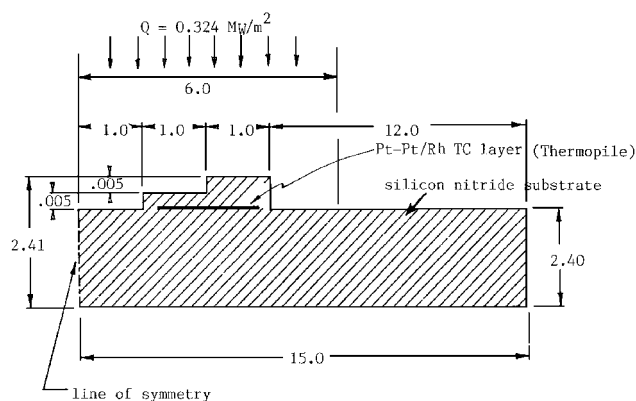

Fig. 10 Heat flux gauge model used for numerical simulation; units: millimeters (not to scale).
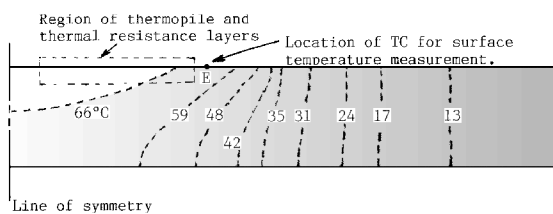

Fig. 11a Temperature profile in the entire heat flux gauge when $t = 1.0$ s and $Q = 0.324$ MW/m^2; temperature units: °C.
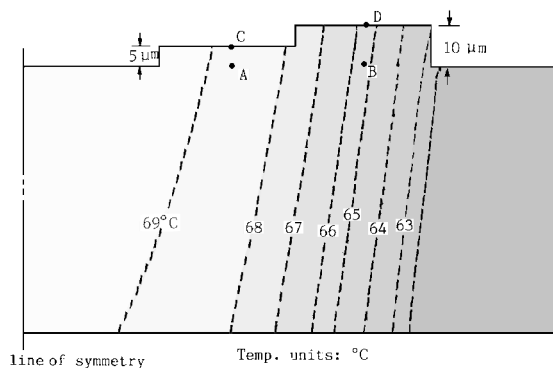

Fig. 11b Enlarged view of the temperature profile near thermopile tip locations A and B, time $t = 1.0$ s, and $Q = 0.324$ MW/m^2; geometry: not to scale.

The temperatures at the surface of the thermal resistance layer, which were directly above A and B, were designated C and D. According to the FLUENT data files, the temperatures at A, B, C, and D were 68.41, 65.86, 68.48, and 65.99°C, respectively.

This indicates that the delta-T across the 5-μm-thick thermal barrier between A and C was 0.07°C. Similarly, delta-T across the 10-μm thermal barrier between B and D was 0.13°C. The temperature difference in radial direction between A and B was 2.55°C. It supports the assumption that the large temperature gradient was created in the radial direction. The temperature difference across the thermal resistance layer is small but a main contributing term in the transient temperature response characteristic. Because there is no distortion in the temperature profile near the Pt–Pt/Rh thermopile region, the effect of radial heat conduction through the thermocouples can be neglected.

Delta-T was computed with respect to the time until $t = 200$ s and plotted in Fig. 8a. Compared with the actual experimental results, the computational results show a reasonable agreement.

Frequency Response of the Heat Flux Gauge

The next test was to evaluate the dynamic response characteristics of the thin-film heat flux gauge. As shown in Fig. 7, an ultra-fast-response Hg–Cd–Te infrared detector was installed to measure the incoming laser pulse frequency. According to the manufacturer, the detector had a high-frequency response of 800 kHz. For the test,
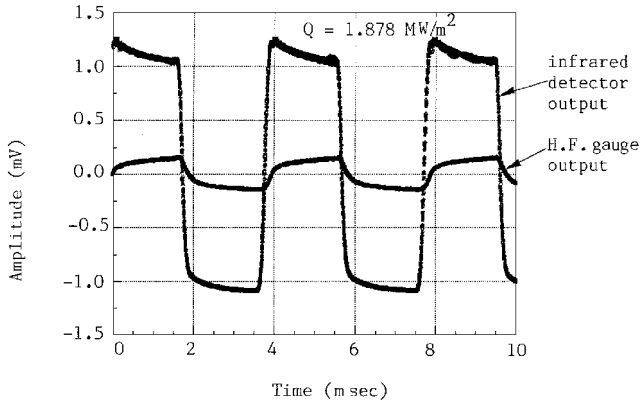
Fig. 12 Frequency responses of the infrared detector and the heat flux gauge, chopper frequency = 250 Hz, nonamplified signals.
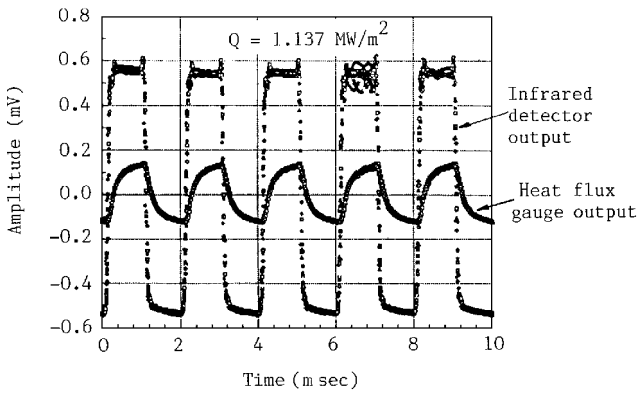

Fig. 13 Frequency responses of infrared detector and the heat flux gauge, chopper frequency = 500 Hz, nonamplified signals.

4% of the laser beam was split and directed toward the Hg–Cd–Te detector and the rest of the laser beam was directed to the heat flux gauge.

During the test, the laser beam diameter of 6 mm was used without beam expansion. A pulse laser beam was artificially generated by a mechanical chopper. The chopper was operated at speeds of 0–6000 rpm. Two types of chopper wheels, which had four apertures and six apertures, were used. The chopper's frequencies were adjusted to create the chopping frequencies of 250 and 500 Hz.

The infrared detector output was assumed to represent the characteristics of the incoming pulse laser beam because of the detector's ultra-high-frequency-response capability. Signal outputs from the heat flux gauge and the infrared detector were both sent through the antialiasing filter, the amplifier, and an A/D data acquisition system.

The raw data without amplification were collected at the chopper frequencies of 250 and 500 Hz and are shown in Figs. 12 and 13, respectively. If it is needed, the thermopile output voltage can be converted to the corresponding temperature using the S-type thermoelectric table. In Figs. 12 and 13, the dc components of the signal were removed through high-pass filters. As shown in Fig. 13, the detector's response was much sharper than that of the heat flux gauge. During the chopping period, the slope of the detector output was very steep and close to a vertical line. In contrast, the signal output from the heat flux gauge was in the form of an alternating exponential curve.

To find the frequency response characteristic of the heat flux gauge, 1024 data points were analyzed using the fast Fourier transform (FFT) technique. The chopper's frequency is the fundamental frequency in the frequency spectrum. Amplitudes obtained from the FFT analysis are used to determine the amplitude ratio.

The nondimensional amplitude of the infrared detector is calculated from the FFT results by dividing the harmonic amplitude by the amplitude of the fundamental. The nondimensional amplitude of the heat flux gauge is calculated similarly. Finally, the nondimensional amplitude ratio was calculated from the nondimensional heat flux

Table 1 Test conditions for the frequency response tests

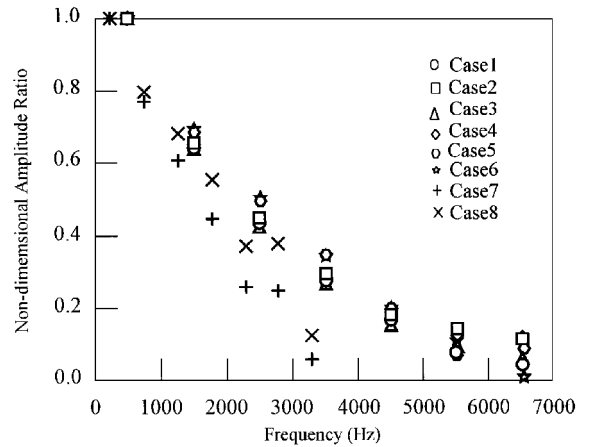| Case no.	Laser power Q, MW/m^2	Sampling rate, kHz	Sampling period, s	Chopper frequency, Hz
1	1.621	40	2	500
2	1.878	40	2	500
3	1.137	40	2	500
4	2.281	40	2	500
5	1.878	100	1	500
6	1.313	100	1	500
7	1.878	100	1	250
8	0.946	100	1	250

Fig. 14 Frequency response characteristic of the heat flux gauge for the test cases in Table 1.
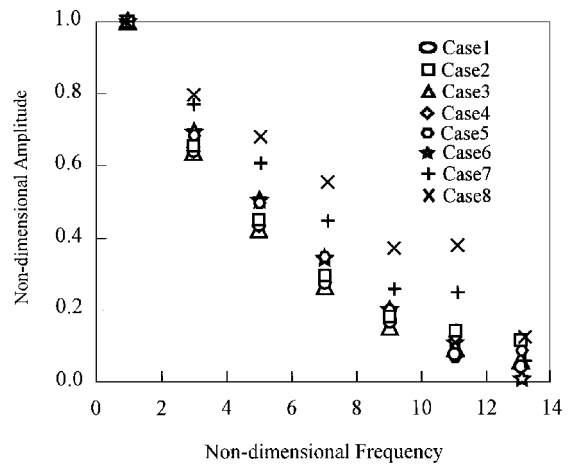

Fig. 15 Nondimensionalized frequency response characteristic of the heat flux gauge.

gauge amplitude divided by the nondimensional amplitude of the infrared detector. Tests were performed at different power levels and chopper frequencies. These test cases are summarized in Table 1.

The nondimensional amplitude ratios for eight different test cases are plotted in terms of frequency in Fig. 14. To investigate the generalized dynamic response characteristic, all of the test cases are plotted with respect to the nondimensionalized variables, as shown in Fig. 15. The abscissa variable is the nondimensional frequency, the harmonic frequency divided by the fundamental frequency. The frequency response characteristic of the heat flux gauge is decided at the 3-dB level measured downward from the nondimensional amplitude ratio of one.

The corresponding nondimensional frequency in Fig. 15 was determined to be 6.5. In terms of the frequency, the dynamic response range of the heat flux gauge is 3 kHz, as can be found in Fig. 14. Therefore, it can be said that the dynamic frequency response range of the newly designed heat flux gauge is about 3 kHz.

Conclusions

A new design of thin-film heat flux gauge was developed and tested. A thermopile of 40 pairs of Pt–Pt/10%Rh thermocouple junctions was deposited on the same plane of the substrate. Over the thermocouples, thermal resistance layers 5 and 10 μm thick were deposited to create a temperature gradient across those layers. Calibration and testing of these gauges were carried out in an arc-lamp calibration facility. The sensitivity of the gauge is presented in terms of the relative conductivity and surface temperature. The heat flux calculated from the gauge output is in good agreement with the value obtained from the precalibrated standard sensor.

The frequency response of the heat flux gauge was measured in the frequency domain using a CO_2 laser and a chopper. The responses from an infrared detector and the heat flux gauge were measured simultaneously and compared. It was found that the thin-film heat flux gauge has a dynamic frequency response of 3 kHz.

The temperature profile in a steady-state condition was calculated using the FLUENT. The two-dimensional temperature profiles show that the temperature across the thermal resistance layers is the main term contributing to the heat flux measurement. The computational results were compared with the experimental results and show fairly good agreement.

Acknowledgment

References

[1]Korkegi, R. H., "Survey of Viscous Interactions Associated with High Mach Number Flight," *AIAA Journal*, Vol. 9, No. 5, 1971, pp. 771–784.

[2]Gardon, R., "An Instrumentation for the Direct Measurement of Intense Thermal Radiation," *Review of Scientific Instruments*, Vol. 24, No. 5, 1953, pp. 366–370.

[3]Kidd, C. T., "A Durable Intermediate Temperature Reading Heat Flux Transducer for Measurements in Continuous Wind Tunnels," Arnold Engineering Development Center, AEDC-TR-81-19, Arnold Air Force Station, TN, 1981.

[4]Bales, E., Bomberg, M., and Courville, G. E., "Building Applications of Heat Flux Transducers," American Society for Testing and Materials, ASTM 885, Philadelphia, PA, 1985.

[5]Consigny, H., "Heat Transfer Measurement Techniques Used in Development at ONERA/CHLAIS-MEUDON," *New Trends in Instrumentation for Hypersonic Research*, NATO Advanced Research Workshop Proceedings, Vol. 6B, 1992, pp. 1–11.

[6]Miller, C. G., "Comparison of Thin-Film Resistance Heat Transfer Gages with Thin-Skin Transient Calorimeter Gages in Conventional Hypersonic Wind Tunnels," NASA TM-83197, 1981.

[7]Kraabel, J. S., Baughn, J. W., and McKillop, A. A., "An Instrument for the Measurement of Heat Flux from a Surface with Uniform Temperature," *Journal of Heat Transfer*, Vol. 102, Aug. 1980, pp. 576–578.

[8]Liebert, C. H., "Miniature High Temperature Plug-Type Heat Flux Gages," NASA TM-105403, April 1992.

[9]Godefroy, J. C., Clery, M., and Gageanat, C., "Thin Film Temperature Heat Fluxmeters," *Journal of Thin Solid Films*, Vols. 193/194, 1990, pp. 924–934.

[10]Will, H., "Fabrication of Thin Heat Flux Sensors," *Proceedings of the Third Health Monitoring Conference for Space Propulsion Systems*, Univ. of Cincinnati Press, Cincinnati, OH, 1991, pp. 348–355.

[11]Bhatt, H., and Fralick, G., "Novel Thin-Film Heat Flux Sensors: Fabrication and Calibration," *Proceedings of Structural Testing Technology at High Temperature—II*, Society for Experimental Mechanics, Bethel, CT, 1993, pp. 88–97.

[12]Simmons, S. G., Hager, J. M., and Diller, T. E., "Simultaneous Measurement of Time-Resolved Surface Heat-Flux and Freestream Turbulence at a Stagnation Point," *Heat Transfer 1990*, Vol. 2, edited by G. Hetsroni, Hemisphere, New York, 1990.

[13]Epstein, A. H., Guenette, G. R., Norton, R. G., and Yuzhang, C., "High-Frequency Response Heat-Flux Gage," *Review of Scientific Instruments*, Vol. 57, April 1986, pp. 639–649.

[14]"100,000 W Arc-Lamp (Model 107), Vortek Industries, Ltd.," *Industrial Research and Development*, Vol. 25, No. 10, 1983, p. 107.

[15]Holanda, R., Anderson, R. C., and Liebert, C. H., "Heat Flux Measurements on Ceramics with Thin Film Thermocouples," NASA TM 106305, Dec. 1993.

[16]Kreider, K. G., "Sputtered High Temperature Thin Film Thermocouples," *Journal of Vacuum Science and Technology A*, Vol. 11, No. 4, 1993, pp. 1401–1405.

[17]Touloukian, Y. S., and Ho, C. Y., "Thermophysical Properties of Selected Aerospace Materials," Thermophysical and Electronic Properties Information Analysis Center, Purdue Univ., West Lafayette, IN, May 1976.

I. E. Vas
Associate Editor